AGN presence correlates independently with both large-scale bar strength and galactic bulge prominence

Izzy L. Garland,[1]★ Henry Best,[1] Tobias Géron,[2] Chris J. Lintott,[3] Brooke D. Simmons,[4] Rebecca J. Smethurst,[3] Mike Walmsley,[2,5] Michal Zajaček,[1] GZ Team,[!] MUNI AGN Team[1]
[1]*Department of Theoretical Physics and Astrophysics, Faculty of Science, Masaryk University, Kotlářská 2, Brno, 611 37, Czech Republic*
[2]*Dunlap Institute for Astronomy and Astrophysics, University of Toronto, 50 St. George Street, Toronto, ON M5S 3H4, Canada*
[3]*Oxford Astrophysics, Department of Physics, University of Oxford, Denys Wilkinson Building, Keble Road, Oxford, OX1 3RH, UK*
[4]*Department of Physics, Lancaster University, Lancaster, LA1 4YB, UK*
[5]*Jodrell Bank Centre for Astrophysics, Department of Physics & Astronomy, University of Manchester, Oxford Road, Manchester, M13 9PL, UK*
[!]*An Institute*

Accepted XXX. Received YYY; in original form ZZZ

ABSTRACT

Supermassive black holes co-evolve with their host galaxies, predominantly via poorly-understood secular (merger-free) pathways. Isolating such pathways presents difficulties. A merger with minimum mass ratio 1:10 results in a bulge component, so identifying merger-free galaxies observationally relies on accurately determined morphologies. Since bulges can also form via secular processes (such as bars), this often leads to incomplete samples, which introduces selection effects. We aim to disentangle the observed correlations between AGN presence with both bar strength and bulge prominence. By controlling for stellar mass, colour and bulge prominence, we investigate whether an AGN–bar correlation is still present at redshift $z \leq 0.1$. Overall, we find an AGN fraction of 27.9 ± 0.8 per cent in strongly barred galaxies, 21.6 ± 0.7 per cent in weakly barred, and 14.5 ± 0.6 percent in unbarred, in agreement with studies not controlling for bulge prominence. Furthermore, we show that, in fixed bins of bulge prominence, the AGN fraction increases with increasing bar strength. In subsamples split by bar strength, the AGN fraction increases with bulge prominence, indicating that AGN presence correlates individually with both bar strength and bulge prominence. This suggests that, despite bars growing bulge components, AGN are linked to both of these morphological components separately.

Key words: galaxies: active – galaxies: bar – galaxies: disc – galaxies: Seyfert

1 INTRODUCTION

The co-evolution of supermassive black holes (SMBHs) with their host galaxies is observed through a number of relations (see Heckman & Best 2014, for a review). Black hole masses have been found to correlate with both bulge properties, such as velocity dispersion and bulge stellar mass (Ferrarese & Merritt 2000; Häring & Rix 2004), and properties of the host galaxy as a whole, such as total stellar mass (Cisternas et al. 2011; Marleau et al. 2013; Simmons et al. 2017).

SMBHs gain most of their mass during periods of rapid growth and accretion, where they are observed as active galactic nuclei (AGN; Shlosman et al. 1989). Therefore, by examining AGN, we can investigate the origins of this co-evolution.

Whilst mergers between two or more galaxies are known to be one source of AGN triggering, simulations have shown that most SMBH growth occurs via secular (i.e., merger-free) pathways (Martin et al. 2018; McAlpine et al. 2020; Smethurst et al. 2023). However, obtaining a pure and complete sample of galaxies with no major mergers in their recent history is highly challenging observationally.

Martig et al. (2012) showed that galaxies with a bulge–to–total mass ratio of less than 0.1 have had no mergers since $z \sim 2$. Thus we could select bulgeless galaxies as a merger-free sample, however this is incomplete, since pseudobulges grow in the absence of mergers (Kormendy & Kennicutt 2004; Kormendy et al. 2010). These look visually very similar to classical bulges, and without careful structural decomposition (Fahey et al., in prep), combined with dynamical analysis (such as via the Kormendy Relation; Kormendy 1977; Hamabe & Kormendy 1987), distinguishing between secularly built pseudobulges and merger-built classical bulges is virtually impossible. Additionally, there is substantial evidence for merger-free formation of classical bulges (Parry et al. 2009; Bell et al. 2017; Gargiulo et al. 2017; Park et al. 2019; Wang et al. 2019; Guo et al. 2020; Du et al. 2021). Thus, removing all galaxies with a bulge from a sample could mean removing a large number of secularly grown bulges.

The other crucial complication that arises when removing galaxies with a bulge component from a sample is that large-scale galactic bars can build up pseudobulges, providing a correlation between bar presence and bulge presence (Shlosman et al. 1989; Kormendy & Kennicutt 2004; Laurikainen et al. 2007; Combes 2009). Thus,

★ Email: garland@mail.muni.cz

removing all galaxies with a bulge component would affect any observed relationship between bars and AGN.

A correlation between AGN presence and bar presence has been found in a number of works (Knapen et al. 2000; Laine et al. 2002; Laurikainen et al. 2004; Coelho & Gadotti 2011; Oh et al. 2012; Alonso et al. 2018; Garland et al. 2023, 2024; Kataria & Vivek 2024). However, due to the challenges in separating AGN emission from that of the host galaxy, the rarity of observationally merger-free disks (those with only a small bulge component), and the rarity of AGN, many of these studies find only a tenuous link. Other studies find no link at all (e.g., Cheung et al. 2015; Goulding et al. 2017). Some studies (e.g., Galloway et al. 2015; Silva-Lima et al. 2022) find a higher AGN fraction in barred galaxies, but not higher levels of AGN activity. Garland et al. (2024) do not exclude all bulgeless galaxies, and instead look at the AGN fraction with bar strength (divided into unbarred, strongly barred and weakly barred) across the disk-dominated galaxy population. In doing so, they show to a $> 5\sigma$ confidence that strongly barred are more likely to host AGN than weakly barred galaxies, which are in turn more likely to host AGN than unbarred galaxies.

It it important to disentangle the bar–bulge connection in order to gain a clear understanding of what causes the switch-on of an AGN. We investigate whether AGN presence correlates exclusively with bulge presence, with bar presence as a proxy (or vice-versa), or whether AGN presence is linked with both bars and bulges separately. We divide a sample of disk-dominated galaxies by bulge prominence, and investigate the AGN fraction in strongly barred, weakly barred and unbarred galaxies at each bulge prominence. This allows us to test the AGN–bulge link at the same time as the AGN–bar link

This paper is structured as follows. In Section 2, we discuss the sample selection. Our results are presented in Section 3, followed by discussion and conclusion in Sections 4 and 5. Throughout this work, we use WMAP9 cosmology (Hinshaw et al. 2013), where we assume a flat Universe, with $H_0 = 69.3\,\mathrm{km\,s^{-1}\,Mpc^{-1}}$ and $\Omega_m = 0.287$, implemented via Astropy (Astropy Collaboration et al. 2013, 2018, 2022) .

2 DATA COLLATION

In order to study the combined effect of galactic bulges and galactic bars on AGN presence, we utilise the Galaxy Zoo: DESI catalogue (GZD; Walmsley et al. 2023a). GZD consists of morphology classifications for 8.7 million galaxies in the DESI Legacy Surveys, arising from a neural network (*Zoobot*; Walmsley et al. 2023b) trained on Galaxy Zoo volunteer votes. We refer the reader to the release paper for a detailed description of the initial catalogue.

To obtain the morphology and activity classifications, we use the catalogue compiled in Garland et al. (2024, hereafter G24). Again, we refer the reader to their paper for a detailed description, but summarise in brief here.

Walmsley et al. (2023a) match GZD to the MPA-JHU SDSS DR7 catalogue (Abazajian et al. 2009) to obtain emission line fluxes, stellar masses and colours (Kauffmann et al. 2003; Salim et al. 2007), and G24 match to NYU-VAGC to obtain k-corrections (Blanton et al. 2005).

In order to select a sample of not-edge-on, not-merging disks, G24 use the GZD model-predicted vote fractions, namely: $f_{\mathrm{smooth-or-featured\_featured-or-disk}} \geq 0.27$, $f_{\mathrm{disk-edge-on\_no}} \geq 0.68$ and $\zeta_{\mathrm{avg}} < 0.3$, where $f_{\mathrm{smooth-or-featured\_featured-or-disk}}$ is the fraction of volunteers who voted for 'featured or disk', as predicted by *Zoobot*, $f_{\mathrm{disk-edge-on\_no}}$ is the model-predicted fraction of volunteers who voted for 'not edge-on', and ζ is the merger prominence parameter. The first two conditions were described in Walmsley et al. (2022), and merger prominence in G24.

Having compiled this initial sample, G24 separate the galaxies into unbarred, weakly barred, and strongly barred. Using the methodology in Géron et al. (2021), a galaxy is designated as unbarred (Ubar) if $f_{\mathrm{strong-bar}} + f_{\mathrm{weak-bar}} < 0.5$. Otherwise it is considered barred. This barred sample is then further split into strong and weak. A galaxy is designated as weakly barred (Wbar) if it is not unbarred, *and* $f_{\mathrm{strong-bar}} < f_{\mathrm{weak-bar}}$. A galaxy is designated as strongly barred (Sbar) if it is not unbarred, *and* $f_{\mathrm{strong-bar}} \geq f_{\mathrm{weak-bar}}$.

To ensure completeness and reduce selection effects, G24 volume-limit the sample, with $z \leq 0.1$, and $M_r \leq -19.2$, as shown in their fig. 1.

Additionally, for this work we require an estimate of the bulge contribution to the galaxy morphology. Masters et al. (2019) define a bulge prominence parameter, B_{avg}, using SDSS morphology classifications from Galaxy Zoo 2 (GZ2; Willett et al. 2013). However, GZ2 had only four different categories of bulge presence: none, just noticeable, obvious, and dominant. GZD divides bulge presence into five categories: none, small, moderate, large and dominant. Thus, we adapt B_{avg} to

$$B = 0.2p_{\mathrm{small}} + 0.5p_{\mathrm{moderate}} + 0.8p_{\mathrm{large}} + 1.0p_{\mathrm{dominant}}$$

where B is the bulge prominence parameter used in this work.

We also use the activity classifications published by G24. The authors divide their sample, via emission-line diagrams (Baldwin, Phillips & Terlevich 1981; Veilleux & Osterbrock 1987), into AGN, star-forming, LINER, composite, undetermined and uncertain. The undetermined galaxies are those who have Hα flux with a signal-to-noise ratio of $\mathrm{S/N_{H\alpha}} < 3$, and thus have neither sufficient star-formation nor AGN activity to make an accurate determination. Visual inspection shows that these undetermined galaxies (in this disk-dominated sample) are predominantly quiescent, red spirals. Uncertain galaxies are those which are lacking sufficient signal-to-noise in other utilised emission lines (Hβ, [O III], [N II], [S II]and [O I]), such that they could theoretically fall into multiple other categories. The LINERs, composites and uncertain galaxies are removed from the sample to avoid contamination. Again, we refer the reader to G24 for a full description of the activity classification procedure, notably their fig. 2.

These cuts to the data result in our final volume-limited sample of 48 702 disk-dominated, not edge-on, not merging galaxies. There are 27 292 unbarred galaxies, 14 357 weakly barred, and 7 053 strongly barred. The median bulge prominence is 0.335, with a mean of 0.350 and a standard deviation of 0.086. There are 3 163 AGN hosts, 28 000 star-forming galaxies, and 561 undetermined galaxies.

3 RESULTS

We first look at the spread of parameters thought to correlate with bar presence, and AGN presence: stellar mass, $(g-r)_0$ colour (where the 0 indicates correction for galactic absorption), and bulge prominence. The distributions are shown in Fig. 1. Note that we only show the strong and unbarred, and AGN and star-forming distributions in order to avoid crowding the plot, however the inclusive figure with all subsets is shown in the appendix.

As expected, the barred samples tend to lie at a higher stellar mass (M_*), redder colour, and higher bulge prominence (B) than their unbarred counterparts, in agreement with previous studies (e.g., Masters et al. 2011). The AGN hosts also lie at a higher M_*, redder

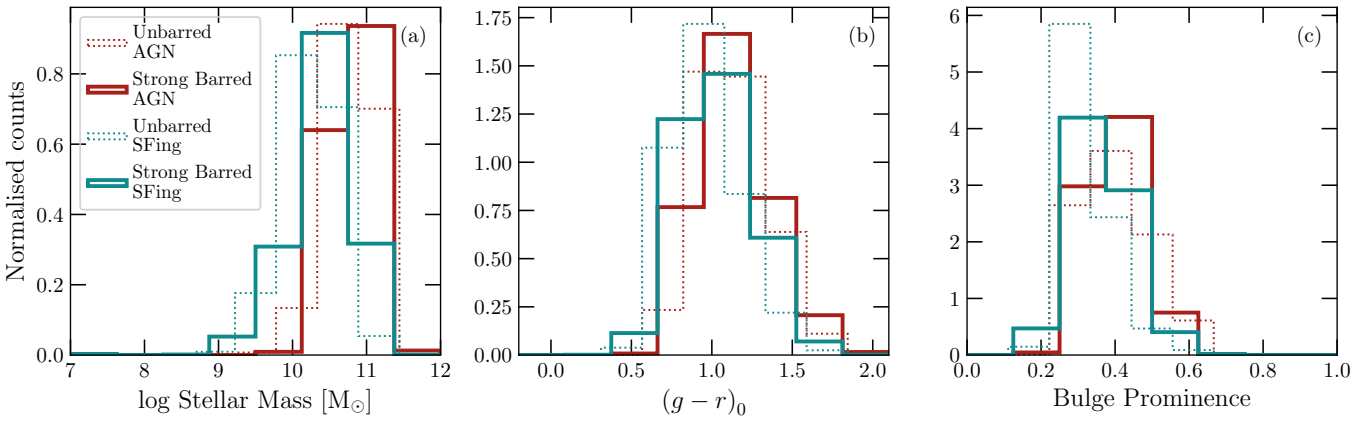

Figure 1. The distributions of stellar mass, Panel (a), $(g-r)_0$colour, Panel(b) and bulge prominence, Panel (c), split into strongly barred galaxies (solid lines), unbarred galaxies (dotted lines), AGN hosts (red) and star-forming galaxies (teal). The star forming galaxies tend to lie at a lower stellar mass, a slightly bluer colour, and a slightly lower bulge prominence than the AGN hosts. The barred galaxies tend to lie at a higher stellar mass, redder colour, and higher bulge prominence than the unbarred subsample.

colour and higher B than the the starforming galaxies, highlighting the need to carefully consider these parameters when investigating an AGN–bar link. This is in line with the general consensus that AGN lie in more massive, redder galaxies (Kauffmann et al. 2003), however, as Aird et al. (2012) points out, this could just be that AGN are more easily observable in more massive galaxies.

This difference in bulge prominence between the AGN and star-forming samples makes isolating the effect of bars on AGN presence non-trivial, since the transport of gas to the centre of galaxies by a bar can cause a pseudobulge to build up (Kormendy & Kennicutt 2004; Laurikainen et al. 2007; Combes 2009). However, by controlling the bulge prominence in much the same way as M_* and $(g-r)_0$, we can investigate whether barred samples still appear to have a higher AGN fraction than unbarred. This can help us determine whether the observed higher AGN fraction in barred galaxies is due to, or independent of, the bulge. Conversely, we can determine if the higher bulge prominence in AGN hosts is due to, or independent of, the bar presence.

In order to account for the difference in M_*, $(g-r)_0$ and B, we control for these three parameters. We divide our sample into 15 evenly-spaced bins in M_*(with a range of $7.0 \leq \log(M_*/\mathrm{M}_\odot) \leq 12.0$), 15 bins in $(g-r)_0$ (with a range of $0.4 \leq (g-r)_0 \leq 2.0$), and 10 bins in B (with a range of $0 \leq B \leq 1.0$). From here, we assign weights to each galaxy, such that the distributions of these three parameters are the same between the SBAR, WBAR and UBAR subsamples. This extends the work of G24, who only controlled for M_* and $(g-r)_0$.

We then look at the overall AGN fraction (f_{AGN}) in each of the bar subsamples. These results are shown in Fig. 2, and Table 1. After controlling for M_*, $(g-r)_0$ and B, the AGN fraction in strongly barred galaxies is greater than that in weakly barred galaxies, which is greater than in unbarred galaxies, and all of these are to $> 3\sigma$ confidence.

Whilst the overall trends agree with those of G24, the quantitative results differ slightly. This is to be expected, however the quantitative results are still in agreement to 3σ. This work has marginally smaller errors, differing from G24 by a maximum of 0.1 percentage points. This highlights that controlling for bulge prominence could increase the accuracy of the AGN fractions, but not significantly on this scale.

In order to further disentangle the apparent three-way link between AGN presence, bulge prominence and bar presence, we investigate the AGN–bar link in bins of B. Using the controlled sample described above, we divide our sample into 10 evenly spaced B bins of width 0.1. Within each of these bins, we calculate the AGN fraction in strongly barred, weakly barred and unbarred galaxies. The results are shown in Fig. 3.

We only plot the bins where there are a minimum of 5 AGN in a bulge prominence bin after weighting to reduce noise.

In each B bin, we see the same overall trend of strongly barred galaxies having a higher incidence of AGN than weakly barred galaxies, which have a higher incidence than unbarred galaxies. The shaded regions represent 2σ errors. At particularly high and particularly low bulge prominence, the errors are greater, likely due to lower numbers of galaxies. However, for the first three bins, the bar-strength–AGN trend is seen to 1σ, and for the bin centred on $B = 0.35$, this result is seen to 3σ. We also see the AGN fraction increase in each bar strength category with bulge prominence – there is a higher fraction of AGN in subsamples with a more prominent bulge component.

In order to further hone in on the driver(s) of these correlations, we investigate how the AGN fraction in each bar category varies across colour–mass–bulge-prominence space. We divide our sample into 10 M_* bins, 10 $(g-r)_0$ bins and 10 B bins, to give 1000 bins. We ignore any bins with less than 10 AGN, in order to reduce noise. In each remaining bin, we calculate the difference between the fraction of strongly barred galaxies hosting AGN, $f_{\mathrm{AGN,SBAR}}$ and the fraction of unbarred galaxies hosting AGN, $f_{\mathrm{AGN,UBAR}}$. The median difference

Table 1. The percentage of each activity category within each bar classification, as shown in Fig. 2. We have shown the results from G24 for comparison. AGN presence in strongly barred galaxies is around twice as prolific as in weakly barred or unbarred galaxies.

		SBAR	WBAR	UBAR
This work	AGN	27.9 ± 0.8	21.6 ± 0.7	14.5 ± 0.6
	SF	67.9 ± 0.9	75.4 ± 0.7	83.4 ± 0.6
	Undet	4.2 ± 0.4	3.0 ± 0.3	2.0 ± 0.2
G24	AGN	31.6 ± 0.9	23.3 ± 0.8	14.2 ± 0.6
	SF	63.6 ± 0.9	73.6 ± 0.8	83.9 ± 0.6
	Undet	4.7 ± 0.4	3.1 ± 0.3	1.9 ± 0.2

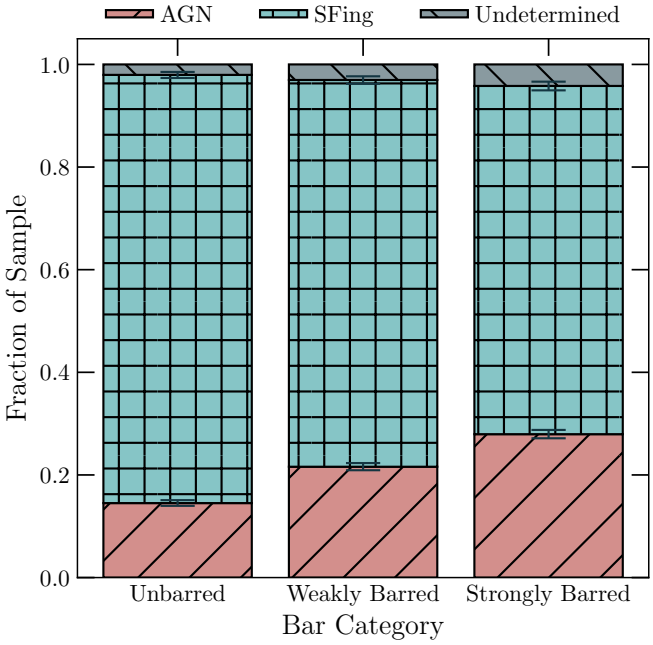

Figure 2. The fraction of AGN, star-forming galaxies and undetermined galaxies in each category of bar strength, as shown in Table 1, after controlling for stellar mass, $(g-r)_0$ colour and bulge prominence. The AGN fraction is shown as red, positive diagonal hatching, star-forming in teal, square hatching and undetermined (i.e., red spirals) in grey negative diagonal hatching. In each case the AGN fraction is smaller than the inactive fraction, however with increasing bar strength, the AGN fraction increases.

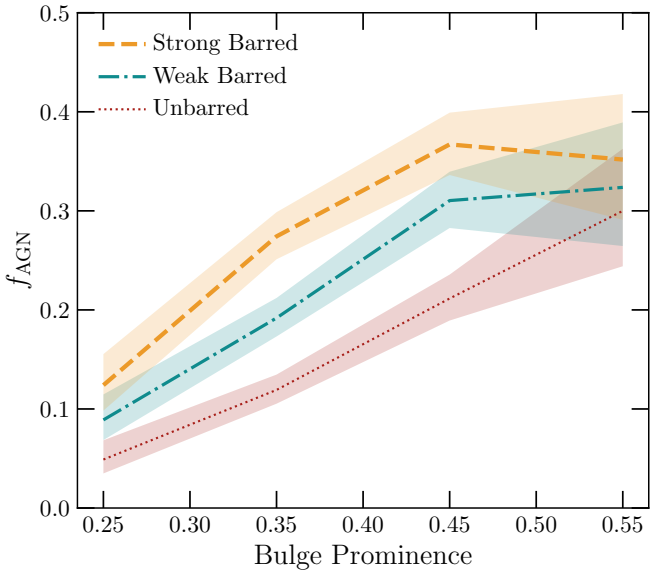

Figure 3. The effect of bulge prominence on AGN fraction, split by bar strength. Strongly barred galaxies are shown in orange, dashed lines, weakly barred in teal, dot-dashed lines and unbarred in red, dotted lines. The shaded regions represent 2σ errors. As bulge prominence increases so does AGN fraction, but AGN fraction also increases in each bulge prominence bin with bar strength.

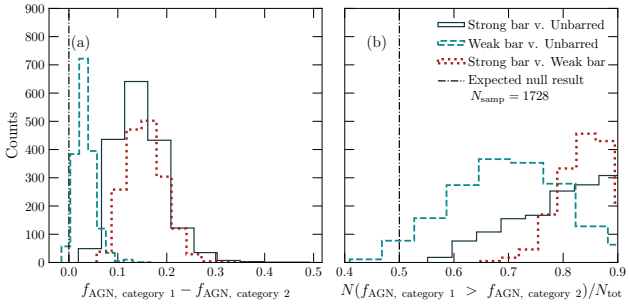

Figure 4. Panel (a): the distributions of the median difference between AGN fractions. Panel (b): the distribution of the fraction of bins where Category 1 bars are more likely to host an AGN than Category 2. In each case, the legend is written as 'Category 1 v. Category 2'. The black dash–dotted lines indicate the expected mean of the distributions if bar presence did not affect AGN presence. The navy blue, solid lines represent SBAR v. UBAR. The teal, dashed lines represent WBAR v. UBAR. The red, dotted lines represent SBAR v. WBAR. The further to the left of the expected null result the histograms lie, the greater the tendency for AGNs to lie in bar Category 1 galaxies, (the stronger bar category of the two being compared).

in these fractions across the bins is $med\left(f_{AGN,SBAR} - f_{AGN,UBAR}\right) = 0.140$. We find the fraction of bins where $f_{AGN,SBAR} > f_{AGN,UBAR}$ to be $N_{f_{AGN,SBAR}>f_{AGN,UBAR}}/N_{tot} = 0.754$. This indicates that across the parameter space, strongly barred galaxies are more likely to host AGN than unbarred galaxies.

To ensure that this result is not just dependent on our choice of binning, we vary the number of bins from 5 to 16 in each direction, for a total of 1 728 bin combinations. For each of these combinations, we find $med\left(f_{AGN,SBAR} - f_{AGN,UBAR}\right)$ and $N_{f_{AGN,SBAR}>f_{AGN,UBAR}}/N_{tot}$. We are assuming that there is a true, intrinsic value of each of these, but we get some scatter when we sample it. Thus, by sampling over multiple binning combinations, we should get a distribution that varies around the true value.

We also repeat this for WBAR v. UBAR, and for SBAR v. WBAR. The results for all three bar comparisons are shown in Fig. 4.

For the difference in the AGN fractions, if there was no intrinsic difference, we would expect the distributions to centre around 0 (i.e., there is no average difference between the AGN fractions). For the fraction of bins where the stronger bar category has a higher AGN fraction, if there was no intrinsic difference, we would expect the distributions to centre around 0.5 (i.e., half of the bins have an greater AGN fraction in one category).

However, in all three bar comparisons, for both plots the distributions lie to the right of the null result, indicating that the AGN fraction is higher across the colour–mass–bulge-prominence regime in the stronger bar category. We test the six distributions for Normality using a Shapiro-Wilk test (Shapiro & Wilk 1965). Only one distribution ($N_{f_{AGN,SBAR}>f_{AGN,WBAR}}/N_{tot}$) has a p-value consistent with Normality, $p_{SW} > 0.05$, so for consistency, we determine significance by calculating the number of standard deviations, σ, between the mean and the null result. The results are shown in Table 2.

In each case, the difference with the null result is significant to at least 2σ, but we only see results that differ by greater than 3σ when we compare strong and weakly barred galaxies.

Table 2. The mean, μ and standard deviation, σ for each plot in Fig. 4, and the number of standard deviations, $\#\sigma$ to the null result. In the case of the median difference in the AGN fraction for the two relevant bar categories, $\Delta f_{\rm AGN}$, the null result is 0. In the case of the number of bins where the AGN fraction is greater in the stronger bar category, $N/N_{\rm tot}$, the null result is 0.5. All of the results are significant to 2σ, but only those concerning SBAR v WBAR are significant to $> 3\sigma$.

		SBAR v UBAR	WBAR v UBAR	SBAR v WBAR
$\Delta f_{\rm AGN}$	μ, σ	0.14 ± 0.06	0.033 ± 0.015	0.09 ± 0.03
	$\#\sigma$	2.44	2.19	3.65
$N/N_{\rm tot}$	μ, σ	0.78 ± 0.10	0.67 ± 0.08	0.74 ± 0.0
	$\#\sigma$	2.73	2.19	5.06

4 DISCUSSION

The positive correlations between $f_{\rm AGN}$ and B and between $f_{\rm AGN}$ and bar strength indicate that there is a highly complex interplay between these three features. There is not only one correlation that mimics the other, and AGN presence correlates with both bar strength and bulge prominence independently.

This indicates that AGN can be triggered and/or fuelled both in galaxies with and without a bulge, with there being a higher AGN fraction in galaxies with a bulge. However, at every bulge prominence, there is a higher AGN fraction in strongly barred galaxies. Similarly, AGN can be triggered and/or fuelled in galaxies with strong bars, weak bars or no bars, with there being a higher AGN fraction in strongly barred galaxies. However, at every bar strength, the AGN fraction increases with bulge prominence.

Both of these correlations have been observed before, such as the work of Garland et al. (2024) demonstrating to a high statistical significance that strongly barred galaxies are more likely to host AGN than their unbarred counterparts, and the canonical Häring & Rix (2004) relationship between bulge stellar mass and black hole mass. Simmons et al. (2017) extended the work of Häring & Rix (2004) to disk-dominated galaxies, and found a correlation between total stellar mass and black hole mass. Given that more massive galaxies are more likely to have a substantial bulge component (or exclusively bulge components in the case of elliptical galaxies), it makes sense that we also see the bulge mass–AGN link of Häring & Rix (2004). We do not have SMBH masses, since our sample consists of Type 2, narrow-line AGN, and broad Hα line measurements are needed for reliable SMBH mass estimates. As demonstrated in Fig. 3, this link with AGN and bulge prominence (a rough proxy for bulge mass) is present even when controlling for bar strength, and the link with bar strength is present even when controlling for bulge prominence.

Given that bars can grow bulges over time via funnelling gas into the centre of the galaxy (e.g., Combes 2009), this adds an extra challenge to understanding these complex relationships. Since bars can build up bulges, barred galaxies with little–to–no bulge component likely represent young bars. Thus, where we have a low bulge prominence, and therefore a lower fraction of AGN, this could indicate that a bar needs to be a minimum age before it can funnel enough gas to the centre to trigger the switch on of an AGN. This contradicts studies such as Garland et al. (2023), who indicate that AGN presence is more likely in bars that are too young to have formed a visible bulge. Further work involving measuring the ages of stellar populations in the bar and bulge in AGN hosts could shine some light on this aspect, rather than relying on the prominence of the bulge to estimate bar age.

The other key reason to consider bar age is that bars are often much longer-lived structures than AGN – 10^{9-10} yr for bars (Kraljic et al. 2012; Sellwood 2014) compared to 10^5 yr for AGN phases (Schawinski et al. 2015). Where we see a barred galaxy without an AGN, it could be that the bar *did* trigger an AGN that has since switched off.

It is highly important to consider our selection effects when drawing conclusions. The galaxies used in this sample are part of the DESI Legacy Surveys, which requires that the point-spread function (PSF) of an image in the z-band is a maximum of $1.5''$. At the redshifts of this work ($z \leq 0.1$), this is equivalent to 2.766 kpc. Any bulges or bars smaller than this may not be resolved, and thus will remain undetected. Higher-resolution photometry (e.g., from *HST*, *JWST* or *Euclid*) is required to pick out these smaller components and make more accurate morphology classifications. However, despite the limitation on photometry, Fahey et al. (in prep) showed that samples can be selected from ground-based surveys such as SDSS that are later confirmed to be disk-dominated with *HST* photometry.

5 CONCLUSIONS

We have used the Galaxy Zoo: DESI catalogue first presented in Walmsley et al. (2023a) and the classifications first presented in Garland et al. (2024) to investigate the dual effect of bulge prominence and bar strength on AGN presence. Our key results can be summarised as follows:

- After controlling for bulge prominence, as well as stellar mass and $(g-r)_0$, we find that the AGN fractions in subsamples split by bar strength are in excellent agreement with Garland et al. (2024), where they only controlled for stellar mass and $(g-r)_0$. That is, that strongly barred galaxies have a higher AGN fraction than weakly barred, which have a higher AGN fraction than unbarred.
- When we split our controlled sample into bins of bulge prominence, we find these same trends in each bin of more strongly barred subsamples having a higher AGN fraction.

Further work is required to investigate these AGN that are fuelled in the absence of bulge components or bar components, as well as investigation of the inactive galaxies where there is a bar and/or bulge present. Tracing of the cold gas in these galaxies with respect to the morphological components, as well as the AGN feedback could help to disentangle this picture. With upcoming large scale surveys, such as those conducted by the Vera C. Rubin Observatory and by *Euclid*, larger samples of disk-dominated galaxies can be obtained. This will enable us to further constrain our relationships in the very low bulge prominence regime.

ACKNOWLEDGEMENTS

ILG, HB and MZ have received the support from the Czech Science Foundation Junior Star grant no. GM24-10599M. BDS acknowledges support through a UK Research and Innovation Future Leaders Fellowship [grant number MR/T044136/1]. CJL acknowledges support from the Sloan Foundation. RJS gratefully acknowledges support through the Royal Astronomical Society Research Fellowship. MW is a Dunlap Fellow. The Dunlap Institute is funded through an endowment established by the David Dunlap family and the University of Toronto.

The data in this paper are the result of the efforts of the Galaxy Zoo volunteers, without whom none of this work would be possible.

Their efforts are individually acknowledged at http://authors.galaxyzoo.org.

Funding for the SDSS and SDSS-II has been provided by the Alfred P. Sloan Foundation, the Participating Institutions, the National Science Foundation, the U.S. Department of Energy, the National Aeronautics and Space Administration, the Japanese Monbukagakusho, the Max Planck Society, and the Higher Education Funding Council for England. The SDSS Web Site is http://www.sdss.org/.

The SDSS is managed by the Astrophysical Research Consortium for the Participating Institutions. The Participating Institutions are the American Museum of Natural History, Astrophysical Institute Potsdam, University of Basel, University of Cambridge, Case Western Reserve University, University of Chicago, Drexel University, Fermilab, the Institute for Advanced Study, the Japan Participation Group, Johns Hopkins University, the Joint Institute for Nuclear Astrophysics, the Kavli Institute for Particle Astrophysics and Cosmology, the Korean Scientist Group, the Chinese Academy of Sciences (LAMOST), Los Alamos National Laboratory, the Max-Planck-Institute for Astronomy (MPIA), the Max-Planck-Institute for Astrophysics (MPA), New Mexico State University, Ohio State University, University of Pittsburgh, University of Portsmouth, Princeton University, the United States Naval Observatory, and the University of Washington.

The Legacy Surveys consist of three individual and complementary projects: the Dark Energy Camera Legacy Survey (DECaLS; Proposal ID #2014B-0404; PIs: David Schlegel and Arjun Dey), the Beijing-Arizona Sky Survey (BASS; NOAO Prop. ID #2015A-0801; PIs: Zhou Xu and Xiaohui Fan), and the Mayall z-band Legacy Survey (MzLS; Prop. ID #2016A-0453; PI: Arjun Dey). DECaLS, BASS and MzLS together include data obtained, respectively, at the Blanco telescope, Cerro Tololo Inter-American Observatory, NSF's NOIRLab; the Bok telescope, Steward Observatory, University of Arizona; and the Mayall telescope, Kitt Peak National Observatory, NOIRLab. Pipeline processing and analyses of the data were supported by NOIRLab and the Lawrence Berkeley National Laboratory (LBNL). The Legacy Surveys project is honored to be permitted to conduct astronomical research on Iolkam Du'ag (Kitt Peak), a mountain with particular significance to the Tohono O'odham Nation.

NOIRLab is operated by the Association of Universities for Research in Astronomy (AURA) under a cooperative agreement with the National Science Foundation. LBNL is managed by the Regents of the University of California under contract to the U.S. Department of Energy.

This project used data obtained with the Dark Energy Camera (DECam), which was constructed by the Dark Energy Survey (DES) collaboration. Funding for the DES Projects has been provided by the U.S. Department of Energy, the U.S. National Science Foundation, the Ministry of Science and Education of Spain, the Science and Technology Facilities Council of the United Kingdom, the Higher Education Funding Council for England, the National Center for Supercomputing Applications at the University of Illinois at Urbana-Champaign, the Kavli Institute of Cosmological Physics at the University of Chicago, Center for Cosmology and Astro-Particle Physics at the Ohio State University, the Mitchell Institute for Fundamental Physics and Astronomy at Texas A&M University, Financiadora de Estudos e Projetos, Fundacao Carlos Chagas Filho de Amparo, Financiadora de Estudos e Projetos, Fundacao Carlos Chagas Filho de Amparo a Pesquisa do Estado do Rio de Janeiro, Conselho Nacional de Desenvolvimento Cientifico e Tecnologico and the Ministerio da Ciencia, Tecnologia e Inovacao, the Deutsche Forschungsgemeinschaft and the Collaborating Institutions in the Dark Energy Survey. The Collaborating Institutions are Argonne National Laboratory, the University of California at Santa Cruz, the University of Cambridge, Centro de Investigaciones Energeticas, Medioambientales y Tecnologicas-Madrid, the University of Chicago, University College London, the DES-Brazil Consortium, the University of Edinburgh, the Eidgenossische Technische Hochschule (ETH) Zurich, Fermi National Accelerator Laboratory, the University of Illinois at Urbana-Champaign, the Institut de Ciencies de l'Espai (IEEC/CSIC), the Institut de Fisica d'Altes Energies, Lawrence Berkeley National Laboratory, the Ludwig Maximilians Universitat Munchen and the associated Excellence Cluster Universe, the University of Michigan, NSF's NOIRLab, the University of Nottingham, the Ohio State University, the University of Pennsylvania, the University of Portsmouth, SLAC National Accelerator Laboratory, Stanford University, the University of Sussex, and Texas A&M University.

BASS is a key project of the Telescope Access Program (TAP), which has been funded by the National Astronomical Observatories of China, the Chinese Academy of Sciences (the Strategic Priority Research Program "The Emergence of Cosmological Structures" Grant # XDB09000000), and the Special Fund for Astronomy from the Ministry of Finance. The BASS is also supported by the External Cooperation Program of Chinese Academy of Sciences (Grant # 114A11KYSB20160057), and Chinese National Natural Science Foundation (Grant # 12120101003, # 11433005).

The Legacy Survey team makes use of data products from the Near-Earth Object Wide-field Infrared Survey Explorer (NEOWISE), which is a project of the Jet Propulsion Laboratory/California Institute of Technology. NEOWISE is funded by the National Aeronautics and Space Administration.

The Legacy Surveys imaging of the DESI footprint is supported by the Director, Office of Science, Office of High Energy Physics of the U.S. Department of Energy under Contract No. DE-AC02-05CH1123, by the National Energy Research Scientific Computing Center, a DOE Office of Science User Facility under the same contract; and by the U.S. National Science Foundation, Division of Astronomical Sciences under Contract No. AST-0950945 to NOAO.

DATA AVAILABILITY

The initial GZ DESI data release is available from Walmsley et al. (2023a), and with the activity and morphology classifications used in this work from Garland et al. (2024).

REFERENCES

Abazajian K. N., et al., 2009, ApJS, 182, 543
Aird J., et al., 2012, ApJ, 746, 90
Alonso S., Coldwell G., Duplancic F., Mesa V., Lambas D. G., 2018, A&A, 618, A149
Astropy Collaboration et al., 2013, A&A, 558, A33
Astropy Collaboration et al., 2018, AJ, 156, 123
Astropy Collaboration et al., 2022, ApJ, 935, 167
Baldwin J. A., Phillips M. M., Terlevich R., 1981, PASP, 93, 5
Bell E. F., Monachesi A., Harmsen B., Jong R. S. d., Bailin J., Radburn-Smith D. J., D'Souza R., Holwerda B. W., 2017, ApJ, 837, L8
Blanton M. R., et al., 2005, AJ, 129, 2562
Cheung E., et al., 2015, MNRAS, 447, 506
Cisternas M., et al., 2011, ApJ, 741, L11
Coelho P., Gadotti D. A., 2011, ApJ, 743, L13
Combes F., 2009, in Jogee S., Marinova I., Hao L., Blanc G. A., eds, Astronomical Society of the Pacific Conference Series Vol. 419, Galaxy Evolution: Emerging Insights and Future Challenges. p. 31 (arXiv:0901.0178)

Du M., Ho L. C., Debattista V. P., Pillepich A., Nelson D., Hernquist L., Weinberger R., 2021, ApJ, 919, 135
Ferrarese L., Merritt D., 2000, ApJ, 539, L9
Galloway M. A., et al., 2015, MNRAS, 448, 3442
Gargiulo I. D., Cora S. A., Vega-Martínez C. A., Gonzalez O. A., Zoccali M., González R., Ruiz A. N., Padilla N. D., 2017, MNRAS, 472, 4133
Garland I. L., et al., 2023, MNRAS, 522, 211
Garland I. L., et al., 2024, MNRAS, 532, 2320
Géron T., Smethurst R. J., Lintott C., Kruk S., Masters K. L., Simmons B., Stark D. V., 2021, MNRAS, 507, 4389
Goulding A. D., et al., 2017, ApJ, 843, 135
Guo M., Du M., Ho L. C., Debattista V. P., Zhao D., 2020, ApJ, 888, 65
Hamabe M., Kormendy J., 1987, in de Zeeuw P. T., ed., IAU Symposium Vol. 127, Structure and Dynamics of Elliptical Galaxies. p. 379, doi:10.1007/978-94-009-3971-4_32
Häring N., Rix H.-W., 2004, ApJ, 604, L89
Heckman T. M., Best P. N., 2014, ARA&A, 52, 589
Hinshaw G., et al., 2013, ApJS, 208, 19
Kataria S. K., Vivek M., 2024, MNRAS, 527, 3366
Kauffmann G., et al., 2003, MNRAS, 346, 1055
Knapen J. H., Shlosman I., Peletier R. F., 2000, ApJ, 529, 93
Kormendy J., 1977, ApJ, 218, 333
Kormendy J., Kennicutt R. C., 2004, ARA&A, 42, 603
Kormendy J., Drory N., Bender R., Cornell M. E., 2010, ApJ, 723, 54
Kraljic K., Bournaud F., Martig M., 2012, ApJ, 757, 60
Laine S., Shlosman I., Knapen J. H., Peletier R. F., 2002, ApJ, 567, 97
Laurikainen E., Salo H., Buta R., 2004, ApJ, 607, 103
Laurikainen E., Salo H., Buta R., Knapen J. H., 2007, MNRAS, 381, 401
Marleau F. R., Clancy D., Bianconi M., 2013, MNRAS, 435, 3085
Martig M., Bournaud F., Croton D. J., Dekel A., Teyssier R., 2012, ApJ, 756, 26
Martin G., et al., 2018, MNRAS, 476, 2801
Masters K. L., et al., 2011, MNRAS, 411, 2026
Masters K. L., et al., 2019, MNRAS, 487, 1808
McAlpine S., Harrison C. M., Rosario D. J., Alexander D. M., Ellison S. L., Johansson P. H., Patton D. R., 2020, MNRAS, 494, 5713
Oh S., Oh K., Yi S. K., 2012, ApJS, 198, 4
Park M.-J., et al., 2019, ApJ, 883, 25
Parry O. H., Eke V. R., Frenk C. S., 2009, MNRAS, 396, 1972
Salim S., et al., 2007, ApJS, 173, 267
Schawinski K., Koss M., Berney S., Sartori L. F., 2015, MNRAS, 451, 2517
Sellwood J. A., 2014, Reviews of Modern Physics, 86, 1
Shapiro S. S., Wilk M. B., 1965, Biometrika, 52, 591
Shlosman I., Frank J., Begelman M. C., 1989, Nature, 338, 45
Silva-Lima L. A., Martins L. P., Coelho P. R. T., Gadotti D. A., 2022, A&A, 661, A105
Simmons B. D., Smethurst R. J., Lintott C., 2017, MNRAS, 470, 1559
Smethurst R. J., et al., 2023, MNRAS, p. stad1794
Veilleux S., Osterbrock D. E., 1987, ApJS, 63, 295
Walmsley M., et al., 2022, MNRAS, 509, 3966
Walmsley M., et al., 2023a, MNRAS, p. stad2919
Walmsley M., et al., 2023b, The Journal of Open Source Software, 8, 5312
Wang L., et al., 2019, MNRAS, 482, 5477
Willett K. W., et al., 2013, MNRAS, 435, 2835

This paper has been typeset from a TEX/LATEX file prepared by the author.